Preprint Title Few-photon microwave fields for superconducting transmon-based qudit control

Authors Irina A. Solovykh, Andrey V. Pashchenko, Natalya A. Maleeva, Nikolay V. Klenov, Olga V. Tikhonova and Igor I. Soloviev

Publication Date 02 May 2025

Article Type Full Research Paper

ORCID® iDs Irina A. Solovykh - https://orcid.org/0009-0006-2261-0055; Andrey V. Pashchenko - https://orcid.org/0000-0003-4859-6053; Nikolay V. Klenov - https://orcid.org/0000-0001-6265-3670; Olga V. Tikhonova - https://orcid.org/0000-0003-0229-5992; Igor I. Soloviev - https://orcid.org/0000-0001-9735-2720

Few-photon microwave fields for superconducting transmon-based qudit control

Irina A. Solovykh[1,2], Andrey V. Pashchenko[1,3,4], Natalya A. Maleeva[5], Nikolay V. Klenov*[1,3], Olga V. Tikhonova[1,2,6] and Igor I. Soloviev[1,6, 1, 2, 3, 4, 5, 6]

Address: [1]Lomonosov Moscow State University, Faculty of Physics, Moscow, 119991, Russia; [2]Lomonosov Moscow State University, Skobeltsyn Institute of Nuclear Physics, Moscow, 119991, Russia; [3]All-Russian Research Institute of Automatics n.a. N.L. Dukhov (VNIIA), 127055, Moscow, Russia; [4]Moscow Technical University of Communications and Informatics (MTUCI), 111024, Moscow, Russia; [5]National University of Science and Technology "MISIS", 119049, Moscow, Russia and [6]Kotel'nikov Institute of Radio Engineering and Electronics of RAS, 125009 Moscow, Russia

Email: Nikolay V. Klenov - nvklenov@mail.ru

* Corresponding author

Abstract

Increasing the efficiency of quantum processors is possible by moving from two-level qubits to elements with a larger computational base. An example would be a transmon-based superconducting atom, but the new basic elements require new approaches to control. To solve the control problem, we propose the use of nonclassical fields in which the number of photons is equal to the number of levels in the computational basis. Using theoretical analysis, we have shown that (i) our approach makes it possible to efficiently populate on demand even relatively high energy levels of the qudit; (ii) by changing the difference between the characteristic frequencies of the superconducting atom and a single field mode, we can choose which level to populate; (iii) even the highest levels can be effectively populated in the sub-nanosecond time scale. We also propose the quantum circuit de-

sign of a real superconducting system in which the predicted rapid control of the transmon-based qudit can be demonstrated.

Keywords

Josephson "atoms"; quantum-state-control; superconducting qubits; non-classical fields

Introduction

Currently, quantum computing is under active development, opening new horizons for solving a number of problems that are difficult for classical processors: modeling the behavior of quantum systems, optimization problems, hacking cryptographic systems, solving large systems of linear equations, and analyzing heat conduction equations [1-6].

The basis for the physical implementation of these computations is a quantum processor consisting of computational cells called qudits, whose states can be represented with satisfactory accuracy in the form of a decomposition into n basis states. Today, the main focus is on processors based on qubits (a special case of qudits with n=2) on a superconducting, ionic or other platform. However, it is still not easy to create the necessary number of qubits and control channels to implement really useful quantum algorithms. A promising solution to this problem is to expand the computational basis of an element by switching to qutrits (n=3), ququarts (n=4), and so on [7-12].

We believe that an additional synergistic effect can be achieved by using quantum electromagnetic fields with a comparable (with n) number of photons to control such quantum multilevel systems. The coexistence of different photons in a single waveguide should make it possible to use the scarce control circuits on a quantum chip more efficiently. In the future, the analysis of the behavior of "qudits + multiphoton quantum field" systems will form the basis for the practical implementation of quantum internet and quantum telecommunication systems [13-16].

Among the many possibilities, we will focus on the superconducting platform: it allows to create sources and mixers for microwave photons, qubits and qudits with corresponding characteristic frequencies of transitions between basis states, as well as radiation detectors with the claim of being quantum sensitive [17-23].

So far, the most common artificial atom among the superconducting ones is considered to be a charge qubit with a large shunt capacity, namely a transmon [24-26]. The transmon is technically simple to fabricate, easy to operate, and resistant to decoherence from various sources. The latter feature makes it possible to achieve a long lifetime of this artificial atom (the lifetime of quantum states is tens of microseconds). It should be noticed that the spectrum of eigenvalues of the Hamiltonian of a real transmon (a slightly nonlinear oscillator) is quite close to the equidistant one; however, a number of widely used theoretical models describing its evolution in an external electromagnetic field (the Jaynes-Cummings model) do not take into account the high-lying energy levels of the artificial atom, and even more the nonlinearity existing in a real solid-state system [27-29]. This article presents the results of a theoretical description of the interaction between a few-photon microwave non-classical field and a transmon-based qudit with several even high-lying levels being taken into account. We develop methods of rapid quantum control of designed transmon-based qudit and its state population dynamics. The structure of the article is as follows: first, the model of the system under study is described in more detail, followed by a theoretical description of the Fock-based control of the qudit states and a discussion of possible practical implementations.

Research methods

Model description

The system under consideration consists of a high-quality (the quality factor is about $\approx 10^5 - 10^6$ and depends mainly on external coupling $C_{in/out}$) superconducting resonator connected to a transmon by a capacitance C_g (see Fig.1). The resonator in this system is a quantum harmonic oscillator with a fully equidistant energy spectrum described by bosonic ladder operators $\hat{a}$ and $\hat{a}^+$, and the photon number operator $\hat{n}_a = \hat{a}^+\hat{a}$. The transmon is considered as an anharmonic oscillator (with ladder operators $\hat{b}$ and $\hat{b}^+$) with the number of excitations in the solid-state system similarly introduced as $\hat{n}_b = \hat{b}^+\hat{b}$. In a transmon, the inductance is created using a nonlinear element: a nanoscale Josephson junction, JJ (or a pair of JJs forming an interferometer-like circuit), so the spectrum is no longer equidistant. In the case where the JJ pair is used, the characteristic (plasma) frequency of the transcmon can be quickly adjusted during 10 – 20 ns in the range of 1 GHz by an external magnetic field [30]. In practice, researchers try to reduce the transom frequency dependence on the external magnetic field to get rid of parasitic flux fluctuations. A large shunt capacitance C_B is needed to increase resistance to parasitic charge fluctuations [31].

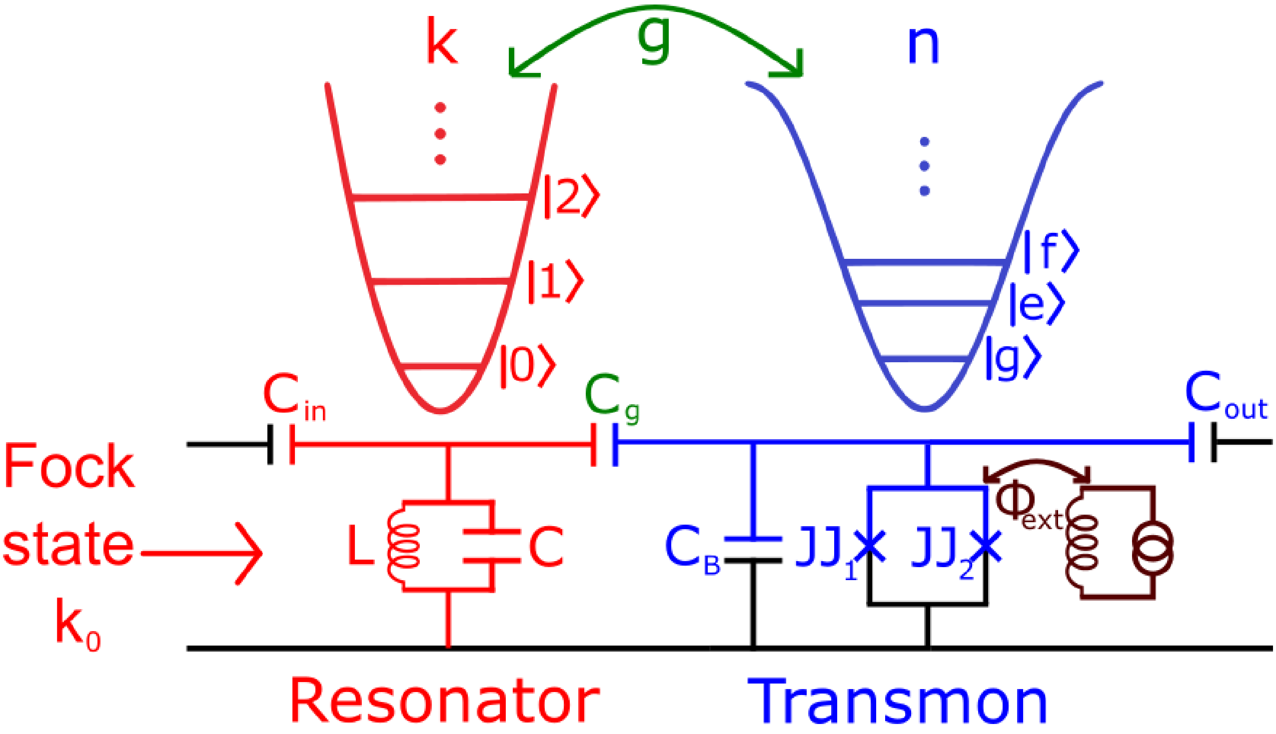

Figure 1: Schematic representation of the model under discussion: few-photon microwave field from a high-quality resonator (red) affect an artificial transmon-based atom (blue). The potential energies and energy spectra for harmonic (resonator) and anharmonic (transmon) oscillators are shown above. Crosses mark the Josephson junctions in the transmon interferometer. The external magnetic flux Φ_{ext} is used to tune the spectrum of a nonlinear system.

A few-photon non-classical microwave field (with a certain number of photons, k_0) enters the resonator [32-36] with variable frequency detuning $\Delta\omega$ between the resonator and the artificial atom. The time evolution of the quantum state of the transmon qudit, the populations of its eigenstates, and the number n of excitations induced in the superconducting system by the quantum field is studied. By taking into account the nonlinearities in the system, it will be shown that there is a certain value of the frequency detuning at which the dynamics of the energy transition from the field to the solid-state system and vice versa is most efficient.

Theoretical description of Fock-based qudit control

First, we need to quantize the field in the harmonic oscillator that corresponds to a high-quality resonator. The energy of the electric field stored in the capacitor and the energy of the magnetic field stored in the inductor can be written as follows:

$$H_{LC} = \frac{Q^2}{2C} + \frac{\Phi^2}{2L} \rightarrow \hat{H}_{LC} = \hbar\omega_0(\hat{a}^+\hat{a} + \frac{1}{2}), \tag{1}$$

with operators of quantum charge and flux introduced by:

$$\hat{Q} = iQ_{zpf}(\hat{a}^+ - \hat{a}), \hat{\Phi} = \Phi_{zpf}(\hat{a}^+ + \hat{a}), \tag{2}$$

where $Q_{zpf} = \sqrt{\frac{\hbar}{2Z_0}}$, $\Phi_{zpf} = \sqrt{\frac{\hbar Z_0}{2}}$ are the vacuum fluctuations of charge and flux, Z_0 is the characteristic impedance, $\omega_0 = \frac{1}{\sqrt{LC}}$ is the resonator angular frequency. The transmon is treated almost the same way, but in this case the number of Cooper pairs on the shunt capacitor C_B (island) and the phase on the JJ/(interferometer) are quantized as follows:

$$\hat{n}_{CP} = \frac{i}{2}(\frac{E_J}{2E_C})^{\frac{1}{4}}(\hat{b}^+ - \hat{b}), \hat{\varphi} = (\frac{2E_C}{E_J})^{\frac{1}{4}}(\hat{b}^+ + \hat{b}), \tag{3}$$

where charge energy $E_C = \frac{e^2}{2C_B}$, Josephson energy $E_J = \frac{\Phi_0 I_c}{2\pi}$ are used (I_c is the critical current flowing through the Josephson junction). The Hamiltonian for the transmon part of our system can be written in the following form, taking into account the nonlinearity [6]:

$$\hat{H}_0 = \hbar\omega_p\hat{b}^+\hat{b} - \frac{E_C}{12}(\hat{b} + \hat{b}^+)^4, \tag{4}$$

where $-\frac{E_C}{12}$ is the nonlinearity parameter, $\omega_p = \frac{\sqrt{8E_J E_C}}{\hbar}$ is the plasma frequency of the transmon. The first term in the Hamiltonian describes a free linear evolution of the photon operators, characterized by their oscillations in time in the Heisenberg representation. The nonlinear term in the Hamiltonian can be averaged over high-frequency oscillations, leaving only smoothly varying terms. This procedure actually corresponds to the so-called Rotating Wave Approximation (RWA), in which the following type of nonlinear term can be obtained:

$$(\hat{b} + \hat{b}^{+})^4 \approx 6\hat{n}_b^2 + 6\hat{n}_b + 3. \tag{5}$$

The expression for the nonlinear term obtained in (5) indicates that the nonlinearity of the transmon is similar to the type of Kerr phase modulation $\gamma\hat{n}_b(\hat{n}_b + 1)$, with $\gamma{=}-\frac{E_C}{2\hbar}$. Thus, the Hamiltonian (4) can be rewritten as follows:

$$\hat{H}_0 = \hbar\omega_p\hat{n}_b + \hbar\gamma\hat{n}_b(\hat{n}_b + 1). \tag{6}$$

Note that for such a system the operator $\hat{n}_b$ is found to be independent on time (being an integral of motion). This means that this nonlinearity itself leads only to phase modulation without changing the excitation statistics.

In our case, the dynamics of the excitations of a Josephson nanosystem (transmon) under the action of a nonclassical electromagnetic field is studied. The interaction of the photonic and superconducting subsystems is investigated by direct solution of the nonstationary Schrodinger equation:

$$i\hbar\frac{\partial\Psi}{\partial t} = \hat{H}\Psi. \tag{7}$$

The Hamiltonian of such a system, taking into account both the nonlinearity of the transmon and the transmon-field coupling, can be written as follows:

$$\hat{H} = \hbar\omega_0(\hat{n}_a + \frac{1}{2}) + \hbar(\omega_0 + \Delta\omega)(\hat{n}_b + \frac{1}{2}) + \hbar\gamma\hat{n}_b(\hat{n}_b + 1) + \hbar\frac{g}{2}(\hat{b}^{+}\hat{a} + \hat{b}\hat{a}^{+}), \tag{8}$$

where $\omega_0 + \Delta\omega = \omega_p$ is the transmon frequency. The interaction strength of the resonator mode with the Josephson subsystem is taken as $g = \frac{d_0\varepsilon_0}{\hbar}$, where $d_0 = 2el(\frac{E_J}{32E_C})^{\frac{1}{4}}$ is the dipole moment of the transmon, $\varepsilon_0 = (\frac{\omega_0}{l})(\frac{C_g}{C_B})\sqrt{\frac{\hbar Z_0}{2}}$ is the vacuum electric field in the resonator that affects the transmon and l is the distance that the Cooper pair travels when tunneling through JJ [37]. The conditions for the application of the rotating wave approximation, which makes it possible to use relation (5), are: $\Delta\omega << \omega_0$ and $g << \omega_0$ [38].

In this paper, the efficiency of the interaction between two subsystems is determined by the average photon density $\frac{<N>}{V_{res}}$, which is large enough to allow field-induced transitions to occur significantly faster than any decoherence processes in the system, which actually corresponds to the strong field regime. This makes it possible to correctly describe the dynamics of a quantum system in terms of the nonstationary Schrodinger equation without taking dissipations into account [39].

The developed theoretical approach appears to be very powerful and allows to describe the mutual influence between the superconducting and field subsystems beyond the perturbation regime with efficient excitation of transmon being taken into account. For the case of few-photons in the field mode the analytical solution of the problem is found. In the general case, the nonstationary Schrodinger equation (7) was solved numerically using the expansion of the total non-stationary wave function in terms of the interaction-free eigenfunctions of the Josephson ϕ_n and field $\tilde{\phi_k}$ subsystems:

$$\Psi = \Sigma C_{n,k}(t)\phi_n\tilde{\phi_k}e^{-\frac{iE_{nk}t}{\hbar}}, \tag{9}$$

with the designation of the total energy in the system $E_{n,k} = \hbar\omega_0(n+\frac{1}{2}) + \hbar\omega_0(k+\frac{1}{2})$. Substituting solution (9) into equation (7) leads to a system of differential equations for probability amplitudes $C_{n,k}(t)$ to find k photons in the field mode and n-fold excitation of the transmon:

$$i\dot{C_{n,k}} = n\Delta\omega C_{n,k} + \gamma n(n+1)C_{n,k} + \sqrt{\frac{n(k+1)}{4}}gC_{n-1,k+1} + \sqrt{\frac{k(n+1)}{4}}gC_{n+1,k-1}. \tag{10}$$

Based on the obtained solution, the probability of detecting a transmon in the state with the number n is given by:

$$P_n(t) = \Sigma_k|C_{n,k}(t)|^2. \tag{11}$$

The probability of finding k photons in the field mode can be found similarly to (11) as follows:

$$W_k(t) = \Sigma_n |C_{n,k}(t)|^2. \tag{12}$$

The initial state is considered to be the Fock state of the resonator with the number of photons k_0 denoted as $\tilde{\phi}_{in} = |k_0\rangle$.

Results

Different regimes of transmon population dynamics

The first feature demonstrated for the interacting superconducting subsystem and a single-mode quantum field is a significant influence of the Josephson nonlinearity (which is similar to the Kerr self-phase modulation) on the dynamics of the transmon excitation.

Figure 2 shows 2D distributions characterizing the time-dynamics of the population of different transmon states in the case of strong and weak nonlinearity in the system. Here we see Rabi-like oscillations [40-42] between different transmon states, and the amplitude of these oscillations is characterized by slow modulation resulting from the nonlinearity effect. It is shown that even a small nonlinearity leads to the appearance of amplitude modulation, and different numbers of states are characterized by different modulation and frequency. Moreover, it is found that significantly different regimes of dynamics take place in dependence on the value of the key-parameter K which combines the characteristics of both effects - the nonlinearity and coupling with quantum field:

$$K = \frac{\gamma k_0(k_0 + 1)}{g}. \tag{13}$$

Actually this parameter represents the ratio between the efficient nonlinearity of transmon and the strength of its coupling with quantum field. And it is very important that the efficient nonlinearity is calculated for maximal possible transmon excitation directly determined by the initial number of photons in the field k_0. For relatively small values of the nonlinearity parameter ($K << 1$), a

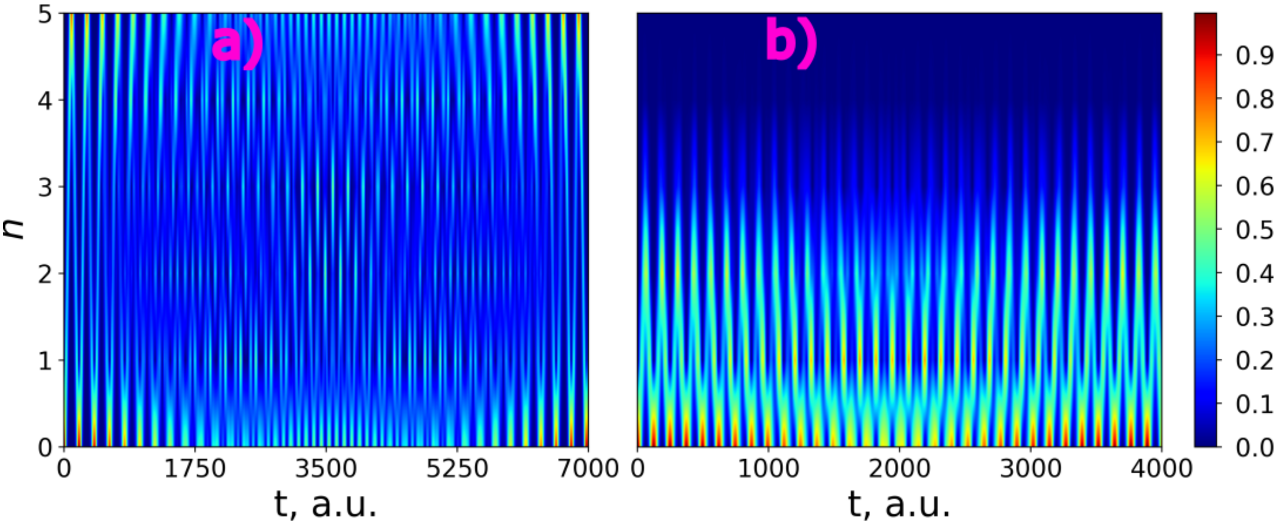

Figure 2: Distribution (colored) of the probability of transmon state excitation versus time with initial state $\psi_{in} = |0\rangle_b|5\rangle_a$ for the case when the nonlinearity parameter (a) $\gamma = -0.001\omega_0$, (b) $\gamma = -0.01\omega_0$ for $g = 0.03\omega_0$, $\Delta\omega = 0$. The dimensionless time unit is t, which is converted to dimensional units with the following formula $\tau = \frac{2\pi t}{\omega_0}$.

strong coupling between the field and the Josephson subsystem gives rise to periodic transition of the transmon to high-energy states, as can be clearly seen in Fig.2(a). Here, all the energy initially stored in the field can be transferred to the transmon with periodic maximal population of the highest possible excited transmon state with $n = k_0$.

In the case of a predominance of nonlinear interaction, high-energy excitation channels are strongly suppressed, as can be seen in Fig.2(b). It was also found that with an increase of the parameter γ, the period of oscillations in channel occupancy increases significantly.

Population control through frequency detuning

As it was shown in the previous Section, the regime of strong nonlinearity when the parameter $K > 1$ leads to suppression of excitation of high-energy transmon states. However, here we propose and discuss a method how to overcome this effect. We have found out that it is possible to controllably manage the excitations in the Kerr nonlinear transmon by varying the frequency detuning of $\Delta\omega$. Using the law of energy conservation in the case of the initial state $\psi_{in} = |0\rangle_b|k_0\rangle_a$, we have analytically found the formula to determine the optimal value of the frequency detuning, that produces the maximum excitation of a certain transmon state "on demand":

$$\hbar\omega_0 k_0 + \langle W_{int}\rangle_{in} = \hbar(\omega_0 + \Delta\omega)n + \hbar\omega_0(k_0 - n) + \hbar\gamma n(n+1) + \langle W_{int}\rangle_{fin}, \quad (14)$$

where $\langle W_{int}\rangle_{in/fin}$ denotes the average value of the interaction energy in the initial and final states of the system, respectively. For an exact number of exitatons in the system, the average interaction energy is zero, which means that for the case of the initial state of the transmon, $\langle W_{int}\rangle_{in} = 0$. In addition, under the condition of ensuring the maximum possible excitation, no energy should be involved in the interaction in the final state, so $\langle W_{int}\rangle_{fin} = 0$. Thus, equality (14) implies an expression for the optimal frequency detuning, at which the maximum excitation of the state with the highest number $n = k_0$ can be achieved:

$$\Delta\omega_{opt_n} = -\gamma(n+1), \quad (15)$$

It should also be emphasized that this analytical method, based on finding the integral of the motion, makes it possible to predict the optimal frequency detuning without solving the system of equation (10). Formula (15) is explicitly confirmed by the numerically calculated 2D probability distribution of the excitation of different transmon states shown in Fig.3 in dependence on frequency detuning and time.

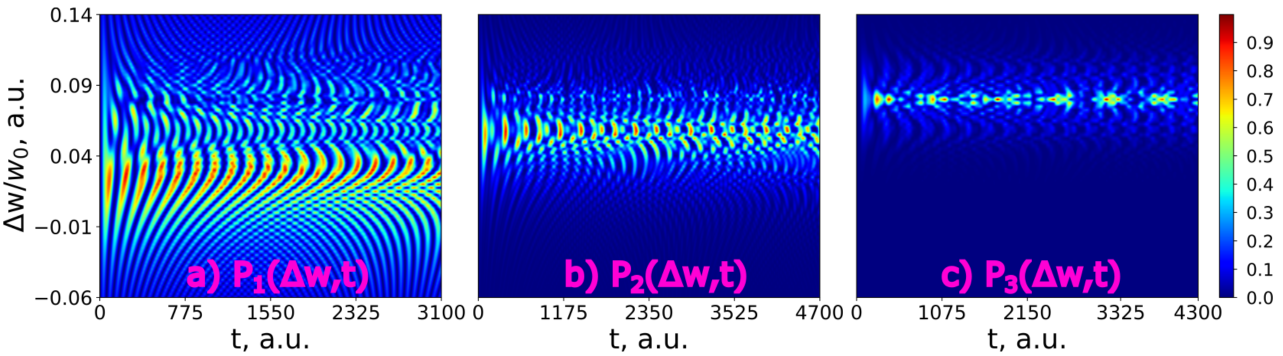

Figure 3: Distribution (colored) of the probability of transmon state excitation versus time of (a) the 1st, (b) the 2nd, and (c) the 3rd of the transmon states at $g = 0.025\omega_0$, $\gamma = -0.02\omega_0$ as a function of the frequency detuning $\Delta\omega$ for the initial state $\psi_{in} = |0\rangle_b|3\rangle_a$.

A very well-pronounced maximum of the probability is found at optimal frequency detuning at each of the three presented distributions. It is important to note that formula (15) is valid and can also be applied in the case of any intermediate transmon state, but in this case the characteristic peak width for the level population can be large enough to lead to some overlapping and interference patterns in the distribution (see Fig.3(a), (b)). Physically, these lateral peaks occur in other settings when not only the desired state is involved in the excitation, but also some other neighbors. In this case, the average interaction energy in (14) becomes non-zero, providing a different energy state that leads to additional preferred values of the frequency detuning.

To demonstrate more precisely the possibility of high-efficient excitation of any transmon state "on demand" by frequency detuning, we calculate the time-dependent populations of transmon levels at optimal points. The results are shown in Fig.4. In the resonance case (Fig.4(a)) the excitation of high energy trasmon states is strongly suppressed due to significant influence of the Kerr nonlinearity ($K = 9.6$). However, it is clearly seen that the frequency adjustments found by formula (15) for the 1st (see Fig.4(b)), 2nd (see Fig.4(c)) and 3rd (see Fig.4(d)) Fock states are indeed optimal values, providing increased excitation of the considered states. The effect of possible maximum excitation is especially pronounced for the highest transmon level when all the input energy of the quantum field is transferred to the superconducting subsystem.

Thus, the optimal frequency detuning allows to overcome the suppression of excitation induced by strong nonlinearity and to achieve periodically maximum population of a certain transmon state "on demand".

Discussion and conclusion: quantum circuit design

The optimal frequency detuning opens the possibility to achieve maximum excitation of a certain transmon state even under strong nonlinearity. In practice, however, the case where K is rather close to unity may be strongly demanded. This regime corresponds to a rather strong coupling between the transmon and the quantum field and can be attractive due to the possibility of much faster transmon dynamics. Moreover, as will be discussed below, the experimental control of the excita-

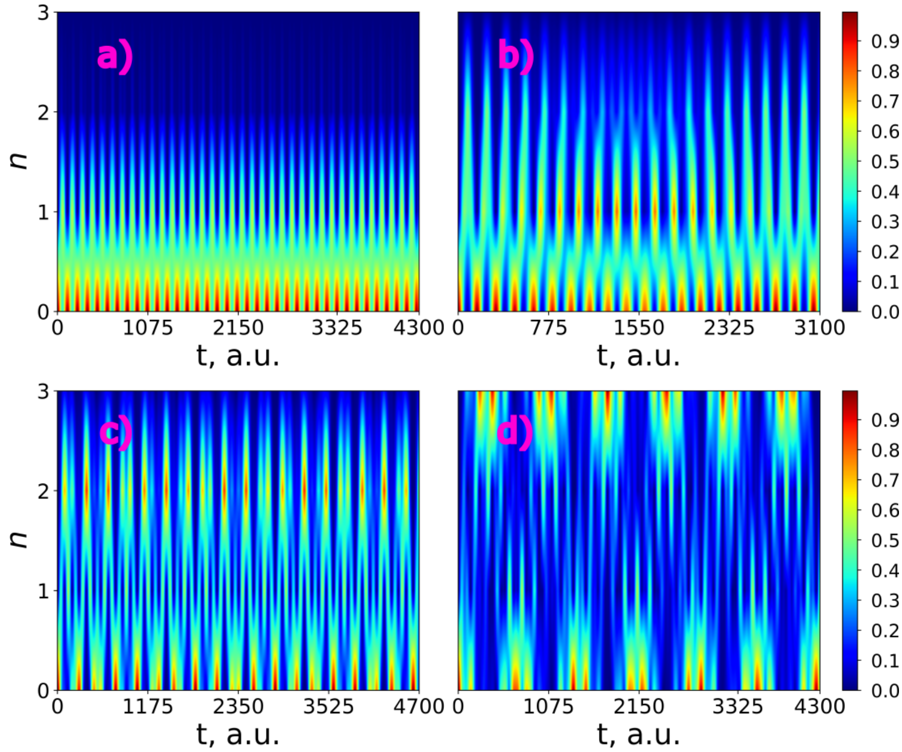

Figure 4: Distribution (colored) of the probability of transmon state excitation versus time obtained in the case of the initial state $\psi_{in} = |0\rangle_b|3\rangle_a$ in the regime of a predominant nonlinear interaction ($K = 9.6$) for $g = 0.025\omega_0$, $\gamma = -0.02\omega_0$ when (a) in resonance case at $\Delta\omega = 0$, (b) at $\Delta\omega = 0.04\omega_0$ - optimal frequency for efficient population of the first state, (c) at $\Delta\omega = 0.06\omega_0$ - optimal frequency for efficient population of the second state, (d) at $\Delta\omega = 0.08\omega_0$ - optimal frequency for efficient population of the third state.

tion is much easier in this case. This regime is difficult to achieve in traditional qubit-based experiments, where everyone deals with the weak coupling regime when $\frac{g}{2\pi} \approx 10$ MHz and $\frac{\gamma}{2\pi} \approx -100$ MHz. Devoret et al. [43] showed that the coupling of the JJ system with the resonator can be significantly enhanced by placing it in the gap of the central conductor of the coplanar waveguide (CPW). In this case, the JJ system will interact directly with the current (magnetic field) in the cavity, and the coupling strength will change from $\frac{g}{\omega_0} \approx \sqrt{\alpha}$ to $\frac{g}{\omega_0} \approx \frac{1}{\sqrt{\alpha}}$, where α is a fine structure constant. This case corresponds to the so-called "ultra-strong coupling regime" [44], which is beyond the scope of this article.

Later, it was shown that this system is inconvenient for practical implementation: the low nonlinearity of $\frac{E_C}{h} \approx 5$ MHz and the huge intrinsic capacitance of JJ $C_J \approx 4$ pcF are difficult to achieve. The reason was that the JJ system was located in the center of the resonator and inductive coupling prevailed. The problem can be solved by using the so-called "in-line transmon" design: one should move the JJ system closer to the edge of the resonator in the area of the maximum voltage in the standing wave, where capacitive coupling will be implemented. At the same time, the value of the coupling strength will decrease, but still remain quite large in comparison to the characteristic nonlinearity $\frac{E_C}{h} \approx 300$ MHz [45,46]. Such a system was further designed as an example to demonstrate the experimental feasibility of the proposed concept for qubit control with microwave photons.

In our case the characteristic magnitude of the nonlinearity $\frac{\gamma}{2\pi} = -\frac{E_C}{2h} = -100$ MHz is directly proportional to the charge energy E_C of the transmon, which is determined by the capacitance of the remaining part of the resonator $l_q = 549$ microns (see Fig.5, the red part of the resonator). The coupling strength can be estimated as:

$$\frac{g}{2\pi} = \sqrt{\frac{2\pi Z_0 \alpha}{Z_{vac}}}(\frac{E_J}{2E_C})^{\frac{1}{4}}\frac{\omega_p}{2\pi}, \qquad (16)$$

and it will vary depending on the external magnetic flux ($E_J(\Phi_{ext})$ and $\frac{\omega_p}{2\pi}(\Phi_{ext})$). Here, $Z_{vac} \approx 377$ Ohms, $Z_0 = 50$ Ohms. Taking this expression into account, at a typical plasma transmon frequency of $\frac{\omega_p}{2\pi} \approx 5-6$ GHz, the coupling strength will be $\frac{g}{2\pi} \approx 1.2$ GHz and efficient state control for qudit will be possible for low energies, $n = 1...3$.

Switching between effectively populated states is carried out when an external magnetic flux Φ_{ext} is applied to the interferometer, taking into account the condition $\Delta\omega_{opt_n} = -\gamma(n+1)$ (see Fig.6). The tuning of plasma frequency is regulated by the interferometric arm asymmetry, and the values of E_J determine the magnitude of the critical current and the area of each JJ: $I_{c1} \approx 39.44$ nA, $S_1 = 200 * 197$ nm; $I_{c2} \approx 22.21$ nA, $S_2 = 149 * 149$ nm with the usual critical current density of $j = 1\frac{\mu A}{\mu m^2}$. The frequency of the resonator was chosen to be $\frac{\omega_0}{2\pi} = 5.348$ GHz to provide simultaneously strong coupling with quantum field and optimal detuning from resonance. In addition, this frequency determines the total length of the system: $2l = 11.101$ mm.

Let's discuss the limitations on the values of the physical parameters in this scheme. First of all,

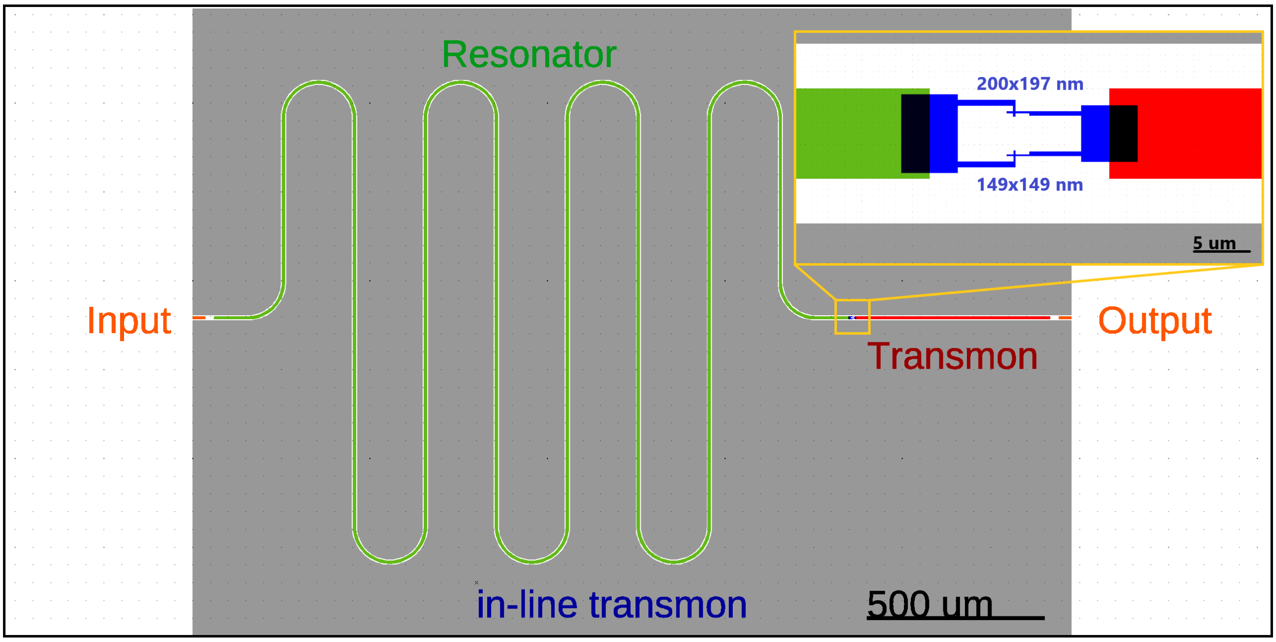

Figure 5: In-line transmon design for efficient transmission of the quantum state: the red part of the central conductor of the resonator and the blue SQUID form a transmon, the total length of the resonator (green and red parts) forms the main resonant mode ω_0.

the following relation between the Josephson and charge energies should be satisfied $E_J >> E_C$, provided in our design by the ratio $\frac{E_J}{E_C} \approx 100$, which correlates well with the chosen type of superconducting artificial atom. The second constraint $C_J << C_s = l_q C^0 << 2lC^0$ is also fulfilled (the capacity JJ can be estimated as $C_J = \varepsilon\varepsilon_0 \frac{S}{d}$, $\varepsilon = 10$, $d = 2$ nm for an AlOx film).

This implementation has a number of significant drawbacks: the system takes up a lot of space on the chip, the impedance matching for the JJ system and the resonator is a problem. Nevertheless, for this discussed in-line transmon design, all necessary parameters are calculated and values of the coupling strength g corresponding to the optimal transmon frequencies predicted by Eq. 15 and providing the most efficient excitation are found for the four lowest transmon states. For each considered transmon state, its population is numerically calculated as a function of frequency detuning and time at the found coupling strength to confirm the designed optimal frequency condition. The results are shown in Fig.7 and obviously prove that the optimal detuning providing maximum excitation of each state explicitly coincides with the value obtained in the designed scheme according

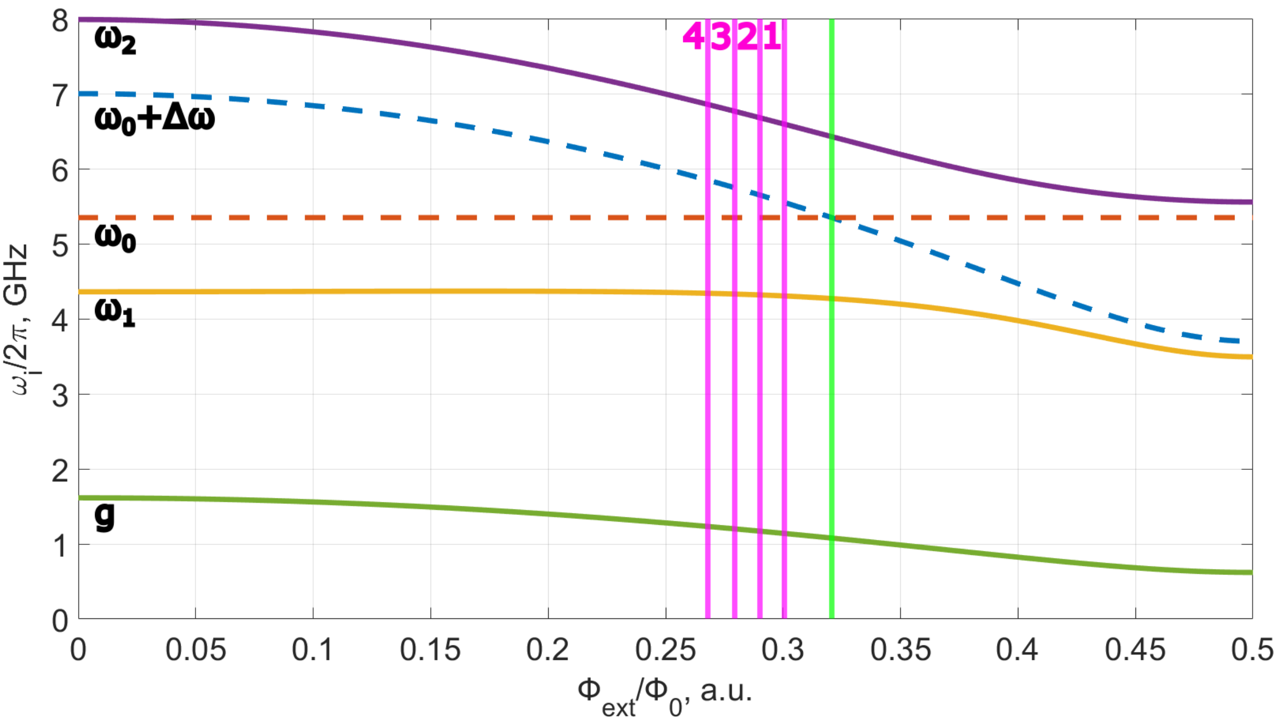

Figure 6: The dependence of the resonator frequency ω_0, the plasma frequency of the qubit $\omega_p = \omega_0 + \Delta\omega$ and coupling strength g between this two systems on the external magnetic flux Φ_{ext}. When these two systems are connected, the united system with two modes ω_1 and ω_2 appears. Anticrossing at the point when the frequencies of the two systems coincide corresponds to the green vertical line.

to formula (15) by varying the external magnetic flux and represented by four pink vertical lines in Fig.6 with corresponding numbers.

Moreover, it can be easily seen that the control of states is very rapid and can be performed on the sub-nanosecond time scale. Indeed, Figure Fig.8 demonstrates the time-dependent probability of excitation of considered transmon states calculated for each state at its own optimal detuning. The obtained results demonstrate a very fast excitation with probability equal to unity achieved for each state of the designed transmon-based qudit, even for the highest one. Thus, the strong coupling regime appears to be very advantageous for the rapid sub-nanosecond control of the designed transmon-based qudit. In this case a very thin tuning to the optimal frequency can be performed by varying the applied magnetic flux.

In conclusion, in this work a fast, simple, and precise control of the population of an artificial atom

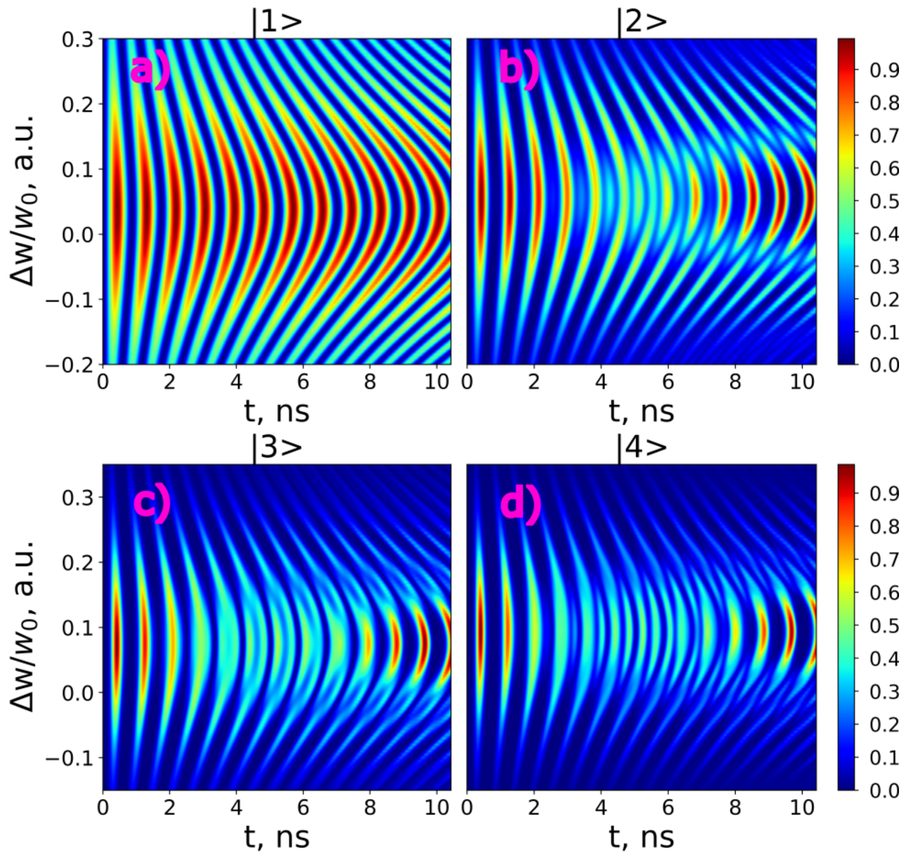

Figure 7: 2D distributions of the populations of states with $n = 1-4$ of the designed transmon with nonlinearity $\gamma = -0.0187\omega_0$ calculated in dependence on frequency detuning and time at certain values of the coupling strength specific for each considered state: a) $g = 0.213\omega_0$, b) $g = 0.219\omega_0$, c) $g = 0.225\omega_0$, d) $g = 0.231\omega_0$. 4 photons are chosen to be initially in the quantum field mode.

is implemented theoretically using microwave photons (Fock states of the resonator). It is important to emphasize that by adjusting the frequency of the nonlinear oscillator (qudit) from the linear resonator mode, we can choose which level of the solid-state subsystem is efficiently populated. In addition, we propose the quantum circuit design of a real superconducting scheme in which the predicted rapid control of transmon-based qudit can be demonstrated. It is important that in a strong coupling regime the efficient transitions in the transmon-based qubit occur on sub-nanosecond timescales [47]. Note that such times are not large in comparison to the decoherence process in the transmon-based qudit [26]. This circumstance makes it possible to design complex fully quantum hybrid "field + solid-state" systems for quantum computing and developing a fully quantum interface between superconducting and photon platforms. From another point of view,

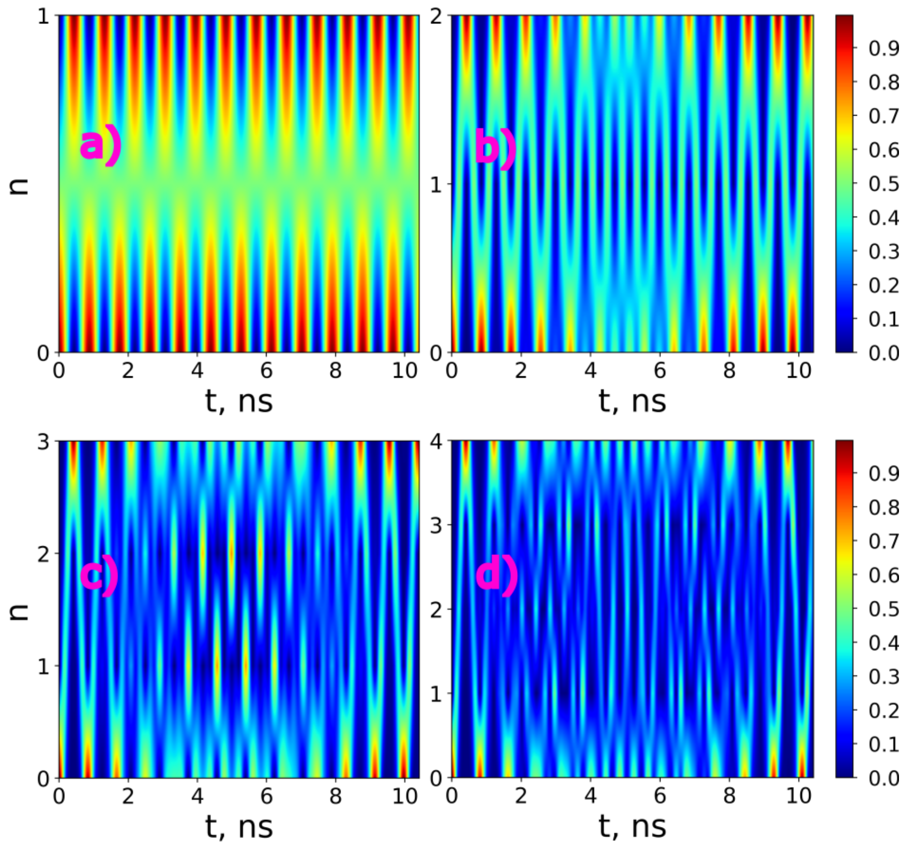

Figure 8: A demonstration of the rapid control of the states with $n = 1 - 4$ of the designed transmon (from (a) to (d), respectively): panels show the time-dependent population of transmon states at the selected optimal frequency detuning. The parameters for each panel are the same as for the corresponding panels in Fig.7.

the developed transmon-based qudit can be used as an electromagnetic field detector, that allows at least to determine the exact number of photons in the resonator.

Acknowledgements

Funding

The study of the basic element for quantum networking is supported by Ministry of Science and Higher Education of the Russian Federation (agreement No. 075-15-2024-538).

References

1. Feynman, R. P. *Foundations of Physics* **1986**, *16*, 507–531.

2. Orús, R.; Mugel, S.; Lizaso, E. *Reviews in Physics* **2019**, *4*, 100028.

3. Kiktenko, E. O.; Pozhar, N. O.; Anufriev, M. N.; Trushechkin, A. S.; Yunusov, R. R.; Kurochkin, Y. V.; Lvovsky, A. I.; Fedorov, A. K. *Quantum Science and Technology* **2018**, *3* (3), 035004.

4. Zhao, L.; Zhao, Z.; Rebentrost, P.; Fitzsimons, J. *Quantum Machine Intelligence* **2021**, *3*, No. 21.

5. Guseynov, N. M.; Zhukov, A. A.; Pogosov, W. V.; Lebedev, A. V. *Phys. Rev. A* **2023**, *107* (5), 052422.

6. Vozhakov, V. A.; Bastrakova, M. V.; Klenov, N. V.; Soloviev, I. I.; Pogosov, W. V.; Babukhin, D. V.; Zhukov, A. A.; Satanin, A. M. *Usp. Fiz. Nauk* **2022**, *192* (5), 457–476.

7. Shnyrkov, V.; Soroka, A.; Turutanov, O. *Physical Review B—Condensed Matter and Materials Physics* **2012**, *85* (22), 224512.

8. Blok, M. S.; Ramasesh, V. V.; Schuster, T.; O'Brien, K.; Kreikebaum, J.-M.; Dahlen, D.; Morvan, A.; Yoshida, B.; Yao, N. Y.; Siddiqi, I. *Physical Review X* **2021**, *11* (2), 021010.

9. Seifert, L. M.; Li, Z.; Roy, T.; Schuster, D. I.; Chong, F. T.; Baker, J. M. *Physical Review A* **2023**, *108* (6), 062609.

10. Kiktenko, E. O.; Nikolaeva, A. S.; Xu, P.; Shlyapnikov, G. V.; Fedorov, A. K. *Physical Review A* **2020**, *101*, No. 2.

11. Liu, P.; Wang, R.; Zhang, J.-N.; Zhang, Y.; Cai, X.; Xu, H.; Li, Z.; Han, J.; Li, X.; Xue, G.; Liu, W.; You, L.; Jin, Y.; Yu, H. *Physical Review X* **2023**, *13*, No. 2.

12. Nikolaeva, A. S.; Kiktenko, E. O.; Fedorov, A. K. *EPJ Quantum Technology* **2024**, *11*, No. 1.

13. Wehner, S.; Elkouss, D.; Hanson, R. *Science* **2018**, *362* (6412), eaam9288.

14. Cacciapuoti, A. S.; Caleffi, M.; Tafuri, F.; Cataliotti, F. S.; Gherardini, S.; Bianchi, G. *IEEE Network* **2019**, *34* (1), 137–143.

15. Kumar, S.; Lauk, N.; Simon, C. *Quantum Science and Technology* **2019**, *4* (4), 045003.

16. Ang, J.; Carini, G.; Chen, Y.; Chuang, I.; Demarco, M.; Economou, S.; Eickbusch, A.; Faraon, A.; Fu, K.-M.; Girvin, S. et al. *ACM Transactions on Quantum Computing* **2024**, *5* (3), 1–59.

17. Zhou, Y.; Peng, Z.; Horiuchi, Y.; Astafiev, O.; Tsai, J. *Physical Review Applied* **2020**, *13*, No. 3.

18. Vozhakov, V.; Bastrakova, M.; Klenov, N.; Satanin, A.; Soloviev, I. *Quantum Science and Technology* **2023**, *8* (3), 035024. doi:10.1088/2058-9565/acd9e6.

19. Pogosov, W. V.; Dmitriev, A. Y.; Astafiev, O. V. *Physical Review A* **2021**, *104*, No. 2.

20. Elistratov, A.; Remizov, S.; Pogosov, W.; Dmitriev, A. Y.; Astafiev, O. *arXiv preprint arXiv:2309.01444* **2023**.

21. Zakharov, R. V.; Tikhonova, O. V.; Klenov, N. V.; Soloviev, I. I.; Antonov, V. N.; Yakovlev, D. S. *Advanced Quantum Technologies* **2024**, *7*, No. 10.

22. Pankratov, A. L.; Gordeeva, A. V.; Revin, L. S.; Ladeynov, D. A.; Yablokov, A. A.; Kuzmin, L. S. *Beilstein Journal of Nanotechnology* **2022**, *13*, 582–589.

23. Chiarello, F.; Alesini, D.; Babusci, D.; Barone, C.; Beretta, M. M.; Buonomo, B.; D'Elia, A.; Gioacchino, D. D.; Felici, G.; Filatrella, G.; Foggetta, L. G.; Gallo, A.; Gatti, C.; Ligi, C.; Maccarrone, G.; Mattioli, F.; Pagano, S.; Piersanti, L.; Rettaroli, A.; Tocci, S.; Torrioli, G. *IEEE Transactions on Applied Superconductivity* **2022**, *32* (4), 1–5.

24. Koch, J.; Yu, T. M.; Gambetta, J.; Houck, A. A.; Schuster, D. I.; Majer, J.; Blais, A.; Devoret, M. H.; Girvin, S. M.; Schoelkopf, R. J. *Physical Review A—Atomic, Molecular, and Optical Physics* **2007**, *76* (4), 042319.

25. Roth, T. E.; Ma, R.; Chew, W. C. *IEEE Antennas and Propagation Magazine* **2022**, *65* (2), 8–20.

26. Wang, Z.; Parker, R. W.; Champion, E.; Blok, M. S. *Physical Review Applied* **2025**, *23* (3), 034046.

27. Houck, A. A.; Schreier, J.; Johnson, B.; Chow, J.; Koch, J.; Gambetta, J.; Schuster, D.; Frunzio, L.; Devoret, M.; Girvin, S. et al. *Physical review letters* **2008**, *101* (8), 080502.

28. Place, A. P.; Rodgers, L. V.; Mundada, P.; Smitham, B. M.; Fitzpatrick, M.; Leng, Z.; Premkumar, A.; Bryon, J.; Vrajitoarea, A.; Sussman, S. et al. *Nature communications* **2021**, *12* (1), 1779.

29. Wang, C.; Li, X.; Xu, H.; Li, Z.; Wang, J.; Yang, Z.; Mi, Z.; Liang, X.; Su, T.; Yang, C. et al. *npj Quantum Information* **2022**, *8* (1), 3.

30. Rol, M. A.; Ciorciaro, L.; Malinowski, F. K.; Tarasinski, B. M.; Sagastizabal, R. E.; Bultink, C. C.; Salathe, Y.; Haandbaek, N.; Sedivy, J.; DiCarlo, L. *Applied Physics Letters* **2020**, *116*, No. 5.

31. Koch, J.; Yu, T. M.; Gambetta, J.; Houck, A. A.; Schuster, D. I.; Majer, J.; Blais, A.; Devoret, M. H.; Girvin, S. M.; Schoelkopf, R. J. *Physical Review A* **2007**, *76*, No. 4.

32. Hofheinz, M.; Weig, E. M.; Ansmann, M.; Bialczak, R. C.; Lucero, E.; Neeley, M.; O'Connell, A. D.; Wang, H.; Martinis, J. M.; Cleland, A. N. *Nature* **2008**, *454*, 310–314.

33. Hofheinz, M.; Wang, H.; Ansmann, M.; Bialczak, R. C.; Lucero, E.; Neeley, M.; O'Connell, A. D.; Sank, D.; Wenner, J.; Martinis, J. M.; Cleland, A. N. *Nature* **2009**, *459*, 546–549.

34. Peng, Z.; De Graaf, S.; Tsai, J.; Astafiev, O. *Nature communications* **2016**, *7* (1), 12588.

35. Dmitriev, A. Y.; Shaikhaidarov, R.; Antonov, V.; Hönigl-Decrinis, T.; Astafiev, O. *Nature communications* **2017**, *8* (1), 1352.

36. Dmitriev, A. Y.; Shaikhaidarov, R.; Hönigl-Decrinis, T.; De Graaf, S.; Antonov, V.; Astafiev, O. *Physical Review A* **2019**, *100* (1), 013808.

37. Blais, A.; Grimsmo, A. L.; Girvin, S. M.; Wallraff, A. *Rev. Mod. Phys.* **2021**, *93*, 025005.

38. Popolitova, D. V.; Tikhonova, O. V. *Laser Physics Letters* **2019**, *16* (12), 125301.

39. Tikhonova, O. V.; Vasil'ev, A. N. *Journal of Physics: Condensed Matter* **2023**, *35* (11), 115301.

40. Johansson, J.; Saito, S.; Meno, T.; Nakano, H.; Ueda, M.; Semba, K.; Takayanagi, H. *Physical Review Letters* **2006**, *96* (12), 127006.

41. Claudon, J.; Zazunov, A.; Hekking, F. W.; Buisson, O. *Physical Review B—Condensed Matter and Materials Physics* **2008**, *78* (18), 184503.

42. Shevchenko, S.; Omelyanchouk, A.; Zagoskin, A.; Savel'Ev, S.; Nori, F. *New Journal of Physics* **2008**, *10* (7), 073026.

43. Devoret, M.; Girvin, S.; Schoelkopf, R. *Annalen der Physik* **2007**, *16*, 767 –779.

44. Andersen, C. K.; Blais, A. *New Journal of Physics* **2017**, *19* (2), 023022.

45. Bourassa, J.; Beaudoin, F.; Gambetta, J. M.; Blais, A. *Physical Review A* **2012**, *86*, No. 1.

46. Hyyppä, E.; Kundu, S.; Chan, C. F.; Gunyhó, A.; Hotari, J.; Janzso, D.; Juliusson, K.; Kiuru, O.; Kotilahti, J.; Landra, A.; Liu, W.; Marxer, F.; Mäkinen, A.; Orgiazzi, J.-L.; Palma, M.; Savytskyi, M.; Tosto, F.; Tuorila, J.; Vadimov, V.; Li, T.; Ockeloen-Korppi, C.; Heinsoo, J.; Tan, K. Y.; Hassel, J.; Möttönen, M. *Nature Communications* **2022**, *13* (1), 6895.

47. Bastrakova, M.; Klenov, N.; Ruzhickiy, V.; Soloviev, I.; Satanin, A. *Superconductor Science and Technology* **2022**, *35* (5), 055003.